Acta Biomaterialia xxx (xxxx) xxx

Contents lists available at ScienceDirect

Acta Biomaterialia

journal homepage: www.elsevier.com/locate/actbio

Full length article

Architecture of β-lactoglobulin coating modulates bioinspired alginate dialdehyde-gelatine/polydopamine scaffolds for subchondral bone regeneration

Farnaz Ghorbani[a,b,c,*], Minjoo Kim[a,d], Behafarid Ghalandari[e], Mingjing Zhang[b], Swastina Nath Varma[b], Lisa Schöbel[a], Chaozong Liu[b,*], Aldo R. Boccaccini[a,*]

[a] Institute of Biomaterials, Department of Materials Science and Engineering, University of Erlangen-Nuremberg, Cauerstrasse 6, 91058 Erlangen, Germany
[b] Institute of Orthopaedic & Musculoskeletal Science, University College London, Royal National Orthopaedic Hospital, Stanmore HA7 4LP, United Kingdom
[c] Department of Translational Health Science, Bristol Medical School, University of Bristol, Bristol BS1 3NY, United Kingdom
[d] Department of Orthopaedics and Trauma Surgery, Musculoskeletal University Center Munich (MUM), LMU University Hospital, LMU Munich, 81377 Munich, Germany
[e] State Key Laboratory of Oncogenes and Related Genes, Institute for Personalized Medicine, School of Biomedical Engineering, Shanghai Jiao Tong University, Shanghai 200030, China

ARTICLE INFO

Article history:
Received 22 January 2024
Revised 21 March 2024
Accepted 15 April 2024
Available online xxx

Keywords:
3D printing
Tissue engineering
Alginate dialdehyde-gelatine
Polydopamine
β-Lactoglobulin

ABSTRACT

In this study, we developed polydopamine (PDA)-functionalized alginate dialdehyde-gelatine (ADA-GEL) scaffolds for subchondral bone regeneration. These polymeric scaffolds were then coated with β-Lactoglobulin (β-LG) at concentrations of 1 mg/ml and 2 mg/ml. Morphological analysis indicated a homogeneous coating of the β-LG layer on the surface of network-like scaffolds. The β-LG-coated scaffolds exhibited improved swelling capacity as a function of the β-LG concentration. Compared to ADA-GEL/PDA scaffolds, the β-LG-coated scaffolds demonstrated delayed degradation and enhanced biomineralization. Here, a lower concentration of β-LG showed long-lasting stability and superior biomimetic hydroxyapatite mineralization. According to the theoretical findings, the single-state, representing the low concentration of β-LG, exhibited a homogeneous distribution on the surface of the PDA, while the dimer-state (high concentration) displayed a high likelihood of uncontrolled interactions. β-LG-coated ADA-GEL/PDA scaffolds with a lower concentration of β-LG provided a biocompatible substrate that supported adhesion, proliferation, and alkaline phosphatase (ALP) secretion of sheep bone marrow mesenchymal stem cells, as well as increased expression of osteopontin (SPP1) and collagen type 1 (COL1A1) in human osteoblasts. These findings indicate the potential of protein-coated scaffolds for subchondral bone tissue regeneration.

Statement of Significance

This study addresses a crucial aspect of osteochondral defect repair, emphasizing the pivotal role of subchondral bone regeneration. The development of polydopamine-functionalized alginate dialdehyde-gelatine (ADA-GEL) scaffolds, coated with β-Lactoglobulin (β-LG), represents a novel approach to potentially enhance subchondral bone repair. β-LG, a milk protein rich in essential amino acids and bioactive peptides, is investigated for its potential to promote subchondral bone regeneration. This research explores computationally and experimentally the influence of protein concentration on the ordered or irregular deposition, unravelling the interplay between coating structure, scaffold properties, and *in-vitro* performance. This work contributes to advancing ordered protein coating strategies for subchondral bone regeneration, providing a biocompatible solution with potential implications for supporting subsequent cartilage repair.

* Corresponding authors.
E-mail addresses: farnaz.ghorbani@bristol.ac.uk (F. Ghorbani), chaozong.liu@ucl.ac.uk (C. Liu), aldo.boccaccini@fau.de (A.R. Boccaccini).

https://doi.org/10.1016/j.actbio.2024.04.028
1742-7061/

Please cite this article as: F. Ghorbani, M. Kim, B. Ghalandari et al., Architecture of β-lactoglobulin coating modulates bioinspired alginate dialdehyde-gelatine/polydopamine scaffolds for subchondral bone regeneration, Acta Biomaterialia, https://doi.org/10.1016/j.actbio.2024.04.028

1. Introduction

Osteoarthritis (OA) is a degenerative disease that affects the cartilage and subchondral bone. Over time, cartilage and underlying subchondral bone wear away and break down, resulting in pain, stiffness, and limited joint mobility [1]. It is essential to address underlying bone structures to repair the joint and effectively relieve osteoarthritis symptoms. In fact, the subchondral bone anchors the collagen fibrils in the adjacent cartilage, which is crucial for joint maintenance [2]. Even though surgical treatment for subchondral bone can effectively reduce pain and improve mobility, it also has several potential disadvantages and risks. A major drawback of surgical treatments is fibrocartilage tissue formation and poor functionality. Additionally, there are risks associated with any surgical procedure, such as infection and blood clots. It is also possible for implants to fail, become loose, dislocate, or break, resulting in the need for revision surgery [3]. Hence, in this context, the focus is on treating subchondral bone defects that arise from OA and restoring function using tissue engineering strategies. The process of osteochondral tissue regeneration is beginning with the formation of a cartilaginous callus within damaged subchondral bone tissue and completing through bone remodelling. This process involves continuous resorption and the formation of bone tissue facilitated by osteoclasts and osteoblasts, respectively [4]. Following this, the development of cartilage tissue commences through chondrocyte cloning and cultivation. As a consequence, the regeneration of subchondral bone is not only necessary to provide mechanical support for subsequent cartilage repair but also plays a pivotal role in ensuring the overall stability and functionality of the joint [5]. Although commercial products for subchondral bone are still in their infancy, some studies have shown that they may reduce pain and improve joint function. Despite the potential benefits of these products, several potential limitations prevent satisfactory outcomes in the repair of large-sized and late-stage defects [6–8].

Additive manufacturing technology can effectively overcome the challenges associated with late-stage OA by developing multi-material and multi-phasic 3D network structures. Its ability to mimic natural tissue architecture, control interconnected pores, fabricate complex shapes, and improve cell growth and internal vascularization, as well as its reproducibility [9] make this technology an excellent choice for developing scaffolds to regenerate subchondral bone defects. Herein, 3D printing of hydrogel is a promising strategy for tissue engineering applications due to hydrogels' biocompatibility, biomimicry, high water content, tuneable mechanical properties, and precise control over structure [10,11]. Alginate dialdehyde (ADA) is a modified form of alginate obtained by oxidizing alginate with a mild oxidizing agent such as sodium periodate to introduce aldehyde groups into the polymer backbone [12], leading to hydrogels with controllable degradation kinetics and enhanced cell interaction [13]. The oxidized alginate can form covalent bonds with amine groups found in proteins or other polymers (such as gelatine) [14]. Gelatine (GEL) is a polymer derived from collagen, a protein found in bone and cartilage. In tissue engineering, gelatine has been extensively studied for its biocompatibility, biodegradability, and ability to form hydrogels. Also, the arginine-glycine-aspartic acid (RGD) sequence in gelatine can promote cell adhesion and migration [15,16]. Although gelatine offers many advantages as a scaffold material, its drawbacks must be addressed to ensure successful clinical translation. Physiological conditions can result in the rapid degradation of gelatine hydrogels, which may limit their durability and stability over long periods [17]. Cross-linked alginate dialdehyde-gelatine (ADA-GEL) offers promising prospects for overcoming this limitation regarding physicochemical, biocompatibility, and cellular interactions.

Mineralization of ADA-GEL scaffolds is essential to subchondral bone repair's structural and mechanical functionality [18]. These polymeric scaffolds exhibit inert properties in forming hydroxyapatite-like layers, making their combination with bioactive agents essential [19]. Herein, surface functionalization of scaffolds with bioactive components is considered an important strategy for tailoring biological functions and bone regeneration. Mussel-inspired polydopamine (PDA), containing abundant catechol and amine groups, possesses several unique properties that make it suitable for various applications, such as bone tissue engineering. PDA is highly adhering to various substrates, is biocompatible, and promotes cell adhesion and proliferation. It also can facilitate hydroxyapatite biomineralization [20,21], as well as being capable of inducing angiogenesis and osteogenesis [22,23]. Accordingly, this nature-inspired polymer has gained significant attention in recent years for the surface functionalization of bone substitutes.

Scaffold surfaces are critical in determining biocompatibility, supporting tissue growth, and interacting with the surrounding tissue. This interaction is mediated by various biomolecules, such as proteins and growth factors [24]. In addition to providing a biocompatible surface, protein coatings can enhance cell adhesion, proliferation, and differentiation. Furthermore, it can improve scaffold structural stability and degradation resistance. Due to the possibility of attaching biomolecules to PDA, it is expected that efficient protein coating of ADA-GEL/PDA scaffolds will occur, assisting the regeneration of bone. Herein, whey protein (50 % β-lactoglobulin and 20 % α-lactalbumin), a milk protein containing a high concentration of essential amino acids and bioactive peptides, has been studied as a potential treatment for bone repair. It is worthy to mention that while bone morphogenic protein-2 (BMP-2), whose recombinant form is predominant in clinical settings [25], is indeed a well-known and extensively studied osteogenic factor, its clinical application needs extensive evaluation due to high cost, potential adverse effects and dose-related complications (inflammation and immune response, ectopic bone formation, soft tissue swelling and seroma formation) [26]. By contrast, β-Lactoglobulin (β-LG) offering advantages in terms of biocompatibility, cost-effectiveness, and sustainability. β-LG's natural presence as a protein within milk endows it with an inherent biological characteristic, rendering it intrinsically biocompatible. Consequently, this property mitigates the likelihood of eliciting adverse immune responses or toxic effects. In a recent study, whey protein enhanced bone-forming cell proliferation and osteogenic differentiation [27]. Accordingly, β-LG-enriched surface is expected to enhance scaffolds' functionality and mechanical fixation, regulate the thermodynamic behaviour of system, and promote cell proliferation and osteogenic differentiation [28,29].

In this investigation, we have developed mono-phasic scaffolds tailored to facilitate the regeneration of subchondral bone, which represents a foundational step in the advancement of osteochondral tissue repair strategies. In our previous research [30], we focused on the fabrication of 3D printed scaffolds using ADA-GEL ink and surface functionalization with polydopamine, followed by an evaluation of the mechanical properties of the scaffolds. Our results indicated that the compressive modulus of the PDA-coated ADA-GEL scaffold (360 $\pm$ 48 MPa) is in the range of subchondral bone compressive modulus of 1–900 MPa [31] that underscores the efficacy of PDA coating in bolstering the mechanical and structural integrity of ADA-GEL scaffolds and indicating promising mechanical properties for load-bearing applications. Given these promising findings, bioinspired PDA functionalized ADA-GEL 3D printed scaffolds were coated with β-LG to promote subchondral bone regeneration. Here, the surface modification with ascending concentrations of protein as well as synergistic cooperation of PDA and β-LG were investigated *in-vitro* and *in-silico*. The purpose was to determine the impact of protein concentration on the deposition

patterns of proteins on scaffold surfaces and thereafter on physicochemical properties as well as cell proliferation and osteogenic differentiation, drawing upon both theoretical models and experimental evidence. The present research confirms that the developed multi-layered scaffolds are promising candidates for regenerating subchondral defects and introduces a new avenue for engineering bi-/multi-phasic scaffolds aimed at osteochondral tissue regeneration.

2. Materials and methods

2.1. Materials

Gelatine from porcine skin (Type A), sodium alginate (sodium salt of alginic acid from brown algae, guluronic acid content 65–70 %), dopamine hydrochloride (Mw = 189.64 g/mol), β-Lactoglobulin from bovine milk, p-Nitrophenyl phosphate (p-NPP), 4′,6-diamidino-2-phenylindole (DAPI), fetal bovine serum, Hank's Balanced Salt Solution (HBSS), and hydrochloric acid (M_w 36.46 g/mol), were purchased from Sigma Co., Germany/United Kingdom. Tris base (Mw = 121.14 g/mol) was purchased from ROTH Co., Germany. Dulbecco's Modified Eagle's Medium (DMEM-low glucose, with 1000 mg/L glucose, L glutamine, and sodium bicarbonate) and bovine serum albumin (lyophilized powder) were purchased from Sigma Co., United Kingdom. Osteoblast differentiation medium was purchased from Cell Applications, Inc., USA. Mouse monoclonal anti-collagen type 1, calcein-AM and propidium iodide, trypan blue, solution penicillin-streptomycin (suitable for cell culture, lyophilized), and PrestoBlue, and BCA protein assay kit were purchased from Thermo Fisher Scientific Co., United Kingdom. Rabbit polyclonal anti-osteopontin, Goat anti-rabbit IgG AlexaFluor 647, and Goat anti-mouse IgG AlexaFlour 488 were purchased from Abcam Biotechnology Co., United Kingdom.

2.2. Preparation of multi-layered scaffolds

ADA-GEL ink was prepared according to previous extensive evaluations [32–34]. Briefly, ink was prepared by gradually mixing equal volumes of ADA solution (resulting in a final concentration of 2.5 % (W/V)) with GEL solution (resulting in a final concentration of 3.75 % (W/V)), leading to Schiff-base reaction of polymers and formation of cross-linked ink with appropriate rheological performance for 3D printing, as extensively studied in our previous investigations [35–38]. The ADA-GEL scaffolds were manufactured using an extrusion-based 3D printer (BioScaffolder 3.1, GeSiM, Großerkmassnadorf, Germany). Scaffolds, structured in a cubic shape (10*10*1 mm^3), was meticulously fabricated utilizing a grid pattern oriented at 0 and 90°. The fabrication process involved the deposition of material in four layers (layer thickness 250 µm) on print bed set at room temperature, employing a precision 250 µm nozzle tip (TIP 25GA TT Precision Tips, Nordson EFD, USA), all executed at 25 ± 1 °C and pressure of 30 kPa. Following this, scaffolds were further cross-linked with 0.6 M $CaCl_2$. Thereafter, 3D printed scaffolds were immersed in dopamine hydrochloride solution (2 mg/mL, pH 8.5) at 37 ± 0.5 °C in the dark. Upon 24 hours of polymerization, the scaffolds were washed with ultrapure water. Uncoated scaffolds were then lyophilized for three days at −54 °C and pressure of 0.001 mbar. These samples are represented by APB0.

Undried ADA-GEL/PDA scaffolds were then coated with β-LG. The β-LG solution was prepared by dissolving the protein in the HBSS at 1 mg/ml and 2 mg/ml concentrations. The scaffolds were then immersed in protein solution for 10 min and were lyophilized for three days after being washed with ultrapure water. The samples APB1 and APB2 correspond to concentrations of 1 mg/ml and 2 mg/ml of β-LG, respectively.

2.3. Physicochemical characterization

The morphology of lyophilized scaffolds was observed using light microscopy (Stemi 508, Carl-Zeiss, Germany) and Field emission scanning electron microscopy (FE-SEM, Auriga, Carl-Zeiss, Germany). Before FE-SEM observation at an accelerating voltage of 3 kV, a thin layer of gold was coated on the samples to obtain a conductive surface. Image measurement software (KLONK Image Measurement Light, Edition 11.2.0.0) was used to measure the pore size and strand diameter.

Chemical characterization of scaffolds was carried out using a Fourier-transform infrared spectrometer (FTIR, IRAffinity-1S, Shimadzu, Japan) with 40 scans in the range of 400–4000 cm^{-1}.

Swelling capacity of scaffolds was determined following the immersion of scaffolds in 10 mL of DMEM cell culture medium. To do this, scaffolds were weighed before and after soaking (incubation in DMEM for 2, 4, 24, and 96 hours at 37 ± 0.5 °C in the dark and speed 60 rpm). The absorption capacity was calculated according to equation 1 [39]:

$$\text{Swelling ratio}(\%) = [(W - W_i)/W_i] * 100 \quad (1)$$

Where W_i is the dry weight of the scaffold, and W is its maximum equilibrated swollen weight.

In-vitro degradation of the scaffolds was evaluated by immersing the scaffolds in 10 mL of DMEM cell culture medium at 37 ± 0.5 °C in the dark and rotational speed 60 rpm. After initial soaking, scaffolds were weighed at 7, 11, 14, and 18-day intervals while the medium was refreshed at each period. Following lyophilisation after 18 days of degradation, the scaffolds were analysed by FE-SEM and FTIR. The degradation ratio of the scaffolds was calculated based on equation 2 [40]:

$$\text{(Bio)degradation ratio}(\%) = |[(W_W - W_i)/W_i]| * 100 \quad (2)$$

Where W_i is the equilibrated swollen weight, and W_w is the wet weight of the scaffolds at a predetermined time interval.

In-vitro bioactivity behaviour was evaluated to determine the biomimetic mineralization of hydroxyapatite-like layers. Scaffolds (10*10*1 mm^3) were incubated in 10 ml of simulated body fluid (SBF) solution for 18 days at 37 ± 0.5 °C and rotational speed 60 rpm. The SBF solution was refreshed every other day. Finally, FE-SEM, FTIR, and XRD analyses were conducted on lyophilized scaffolds. The X-ray diffractometry (MiniFlex 600, Rigaku, Japan) was done in the range of 2θ angles 20–60° using Cu-Kα (λ 1.5418 Å) radiation to evaluate the crystalline structure of mineralized layers.

2.4. Molecular docking calculations

Molecular docking calculations were conducted to investigate β-LG interaction with the PDA surface at different concentrations. Hence, two states regarding the concentration of β-LG were considered as a single molecule (representing low concentration) and a dimer structure (representing high concentration) in this study. The structure of β-LG was acquired from the RCSB with PDB ID: 3NQ9 [41]. According to previous works [23,42], the PDA structure was modelled with a length of 12 repeated-basic units. Then, the PDA geometry was optimized with the AMBER force field implemented in NAMD [43]. The dimer-state was determined based on protein-protein docking calculations and approved taking into account the previous studies [44,45]. HDOCK [46,47] was used to perform molecular docking calculations. VMD package was used to prepare the input files and to analyse the data [48].

2.5. In-vitro *cell studies*

UV-sterilized scaffolds were seeded with 10^5 sheep bone marrow mesenchymal stem cells (sBMSCs)/ml after being soaked in

DMEM for 1 hour to assess cell viability, proliferation, and alkaline phosphatase (ALP) activity. The sBMSCs were obtained from the Institute of Orthopaedic & Musculoskeletal Science at University College London - Royal National Orthopaedic Hospital. Cell-seeded scaffolds were incubated in DMEM supplemented with 10 % FBS and 100 U/ml penicillin-streptomycin and maintained at 37 ± 0.5 °C, 5 % CO_2, and 95 % humidity. Here, a cell culture plate served as a control group. The viability in the control group was set at 100 %, and in the comparison groups, the changes are given as percentage of control.

Following 2 and 7 days of cell seeding, a live/dead staining kit containing Calcein-AM and Propidium Iodide (PI) solutions was used to determine cell viability. Thus, at each time point, the cell culture medium was aspirated, and the scaffolds were incubated for 1 hour at 37 ± 0.5 °C, 5 % CO_2, and 95 % humidity in 2 μM calcein-AM and 4 μM PI in HBSS. Cell viability was studied using a fluorescence microscope (Axio Observer, Carl-Zeiss, Germany) after the constructs were fixed in a fluorescent fix solution.

Proliferation of the cultured cells was measured after 2 and 7 days using PrestoBlue assay. Following removal of the medium at each time point, the cell-cultured samples were incubated in DMEM containing 10 % (V/V) PrestoBlue for 1 h at 37 ± 0.5 °C, 5 % CO_2, and 95 % humidity. The absorbance at 570 nm was then measured using a microplate reader (Infinite M200pro, TECAN, Switzerland).

The osteoblastic behaviour of cultured cells was assessed by measuring ALP activity. After 14 and 21 days of cell culture, cells were lysed with lysis buffer, and the medium was centrifuged at 1200 rpm for 10 min. The supernatant was incubated for 180 minutes with ALP-mix solution containing p-NPP. The reaction was stopped with the addition of NaOH (1M). ALP activity was determined by measuring absorbance at wavelengths of 405 and 690 nm. Finally, BCA protein assay results were used to adjust ALP levels for total protein content.

The expression of osteopontin (SPP1) and collagen type I (COL1A1) was examined using immunocytochemistry. The scaffolds were UV sterilized and seeded with 10^5 human osteoblasts (hOB)/ml after being incubated in osteoblast differentiation medium for 1 h. The hOB cells were obtained from the Institute of Orthopaedic & Musculoskeletal Science at University College London - Royal National Orthopaedic Hospital. Cell-seeded scaffolds were incubated for 21 days in osteoblast differentiation medium at 37 ± 0.5 °C, 5 % CO_2, and 95 % humidity. Media were changed every other day. The cells were then fixed with 4 % (V/V) paraformaldehyde for 10 min and permeabilized with 0.1 % (V/V) triton X-100 for 15 min. Thereafter, cells were blocked with a 2 % (W/V) BSA solution at room temperature. The cells were then incubated overnight at 4 °C with primary antibodies (Mouse monoclonal anti-collagen type 1 (1:100), Rabbit polyclonal anti-osteopontin (1:200)) diluted in 0.1 % (W/V) BSA, and 45 min at room temperature with secondary antibodies (Goat anti-rabbit IgG AlexaFluor 647 (1:1000), and Goat anti-mouse IgG AlexaFlour 488 (1:1000)) diluted in 0.1 % (W/V) BSA. After staining the cells with DAPI (1:1000), they were observed using a confocal laser scanning microscopy (LEICA STP8000, LEICA, Germany).

2.6. Statistical analysis

Each experiment was repeated five times ($n = 5$), and data were reported as the mean±standard deviation. The significance of the average values was calculated using a standard software program (GraphPad Prism version 9.2.0, San Diego, California), and $p \leq 0.05$ was considered significant. ($^{*}P \leq 0.05$; $^{**}P < 0.01$; $^{***}P < 0.001$)

3. Results and discussion

3.1. Microstructural observation

The morphology and microstructure of scaffolds are critical factors that determine biocompatibility and overall tissue responses [49]. The presence of interconnected pores within the scaffold allows for the infiltration of cells and nutrients, promoting tissue ingrowth and integration. A well-defined microstructure facilitates cell–cell and cell–matrix interactions, promoting cell adhesion, migration, and tissue organization [50]. Besides, the surface characteristics of scaffolds, such as surface chemistry and topography, can also facilitate cell adhesion, cell alignment, and promote specific cellular functions [51]. The objective of this study was to modify the surface with osteogenic protein and evaluate its potential for subchondral bone regeneration, as illustrated in Fig. 1. In this study, following functionalization of ADA-GEL scaffolds with bioinspired PDA, they were coated with a layer of protein. Fig. 2(A–I) displays the morphology of the 3D printed scaffolds and those coated with β-LG. Microscopy images reveal the formation of interconnected tubule-like microstructures, showing a well-designed internal structure and desired architecture, facilitating cell infiltration and nutrient transport. The successful functionalization of ADA-GEL scaffolds with spherical PDA particles is evident in FE-SEM images, especially on the edge of printed filaments, demonstrating self-oxidation of dopamine hydrochloride on the surface, which is capable of improving cell adhesion [52]. Also, PDA functionalization on the surface of scaffolds can be visualized by the dark brown colour of the scaffolds, as indicated in our previous publication [30]. The coating of the β-LG on the PDA-functionalized scaffolds is also visible in SEM images. It is expected β-LG coating positively affects osteoblast adhesion, proliferation, and differentiation through formation of a rough surface [53]. Based on FE-SEM images, a relatively uniform and homogeneous coating of β-LG was observed on scaffold surfaces, whereas, following the protein coating and increasing its concentration, a degree of deformation in scaffolds was observed. Coating the proteins on the scaffolds increases the swelling, resulting in a degree of deformation or expansion of the scaffold structure [54]. In addition, the adsorption of proteins can induce conformational changes in the protein molecules [55], impacting the scaffold by exerting mechanical forces that cause deformation or reorganization of the scaffold structure. However, uniform coating of protein highlights the effectiveness of the PDA functionalization strategy in enabling successful β-LG coating onto the scaffold surface, indicating PDA act as an anchor for subsequent β-LG coating [56]. PDA possesses strong adhesive properties due to the presence of catechol and amine functional groups, enabling favourable binding sites for proteins, facilitating their attachment.

According to the average pore size and strand size measurements (Fig. 2(J, K)), the pore size for APB0 was 1150 ± 80 µm and after coating β-LG, this value was reduced to 840 ± 114 µm and 669 ± 90 µm for APB1 and APB2, respectively. Similarly, the average strand thickness was 507 ± 80 µm, 653 ± 142 µm, and 668 ± 125 µm for APB0, APB1 and APB2, respectively. Based on the results, the protein coating resulted in a slight reduction in pore size and an increase in strand diameter; however, the results were not statistically significant. While smaller pore size may enhance certain aspects of cellular activity and tissue ingrowth, it must be within a range conducive to effective biological interactions. It is expected suitable pore size facilitates more selective cell infiltration and the development of organized and functional tissue within the scaffold as well as providing a better support for osteogenesis, mimicking the natural bone matrix, and secretion of extracellular matrix components [57]. The minimal pore dimen-

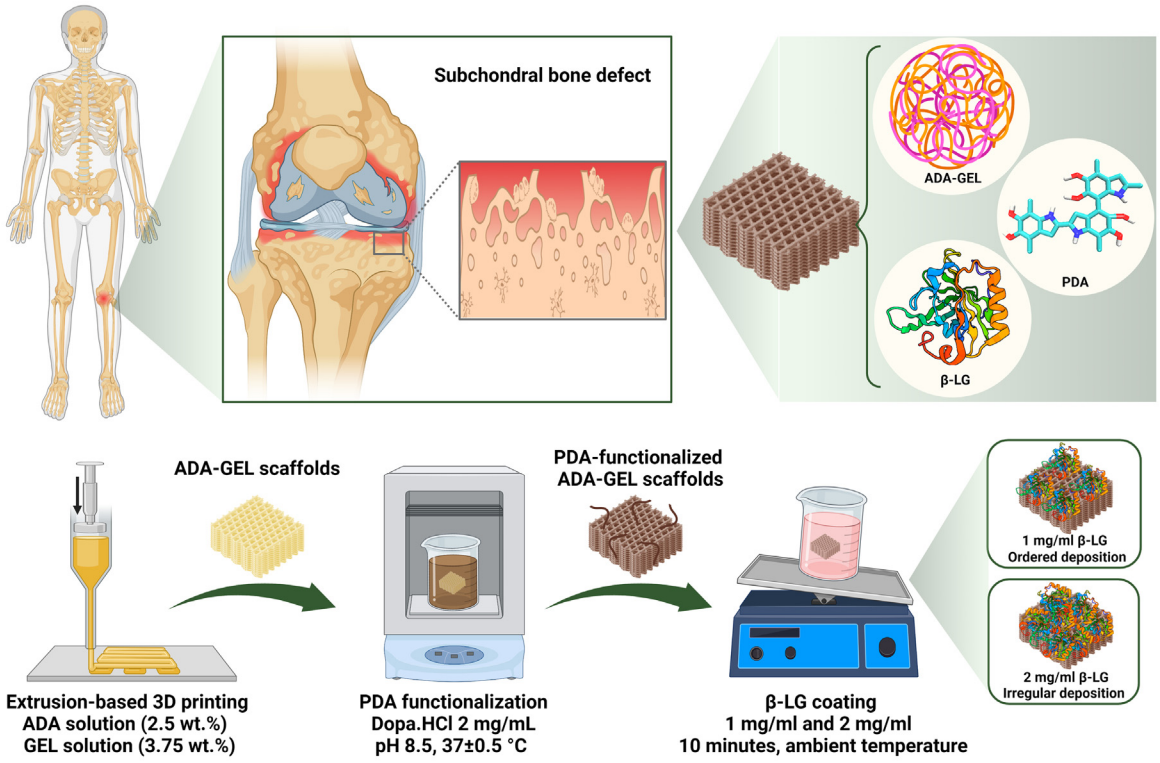

Fig. 1. Schematic illustration of β-LG coated PDA-functionalized ADA-GEL scaffolds for subchondral bone regeneration. (created by www.biorender.com)

sions required to initiate bone ingrowth typically fall within the 100–150 μm range [58,59], primarily due to migration necessities and transport considerations. Nevertheless, pore sizes exceeding 300 μm are suggested as they promote increased new bone formation and capillary development [60]. Other investigation have indicated that pores larger than 900 μm exhibit limited cell bridging capacity [61]. Smaller pores allow for increased surface area, providing more anchorage site for cells and can facilitate stronger interactions between cells and the scaffolds [62]. Zhang et al. [63] engineered porous implants featuring pore sizes ranging from 400 μm to 900 μm. Their findings indicated that pore sizes ranging between 600 and 700 μm yielded promising outcomes for mending bone defects.

3.2. Chemical characterization

Fig. 2(L) presents the FTIR spectra of pure materials and multilayered constructs. For ADA-GEL, the broad peak between 3000 and 3500 cm^{-1} corresponds to hydroxyl functional groups. The peaks at 1600 cm^{-1} and 1414 cm^{-1} corresponds to amide I and II, describing bending and stretching vibrations of the N–H and C–N bonds in the amide groups [35]. For pure synthesized PDA, OH and NH groups in the chemical structure are observed around 1603 cm^{-1} and 1513 cm^{-1}. A broad peak at 3200–3500 cm^{-1} is an indication of stretching vibration of phenolic OH and NH bonds in catechol groups [64]. PDA peaks on APB0 scaffolds confirm the self-oxidative polymerization of dopamine hydrochloride on the ADA-GEL scaffolds. PDA can attach to the surface through both covalent and non-covalent binding mechanisms. Covalent binding happens through Michael-type addition reactions with nucleophilic functional groups in the scaffolds. Additionally, PDA can engage in Schiff base reactions with aldehydes in chemical composition of scaffolds. Non-covalent binding also occurs through hydrogen bonding between the hydroxyl groups of PDA and hydroxyl or carboxyl functional groups of scaffolds. Other non-covalent interactions, including π–π stacking and metal chelating, may also contribute to the attachment of PDA to the ADA-GEL scaffolds [20]. The FTIR peaks at 1626 cm^{-1} and 1525 cm^{-1} show the presence of amide I and amide II bonds in β-LG. The amide III bond appears 1232 cm^{-1} and is associated with the vibrations of N–H and C–N bonds. A minor peak at 1454 cm^{-1} is characteristic of a predominantly β-sheet structure. The peak around 3200 cm^{-1} is attributed to OH in the chemical structure of β-LG [65]. Observation of these peaks in APB1 and APB2 as well as increasing intensity of amide peaks corresponded to coating the scaffolds with ascending concentration of β-LG. PDA and β-LG can interact through covalent and non-covalent bonding, leading to protein immobilization on the surface. One possible interaction can be Schiff base interaction due to the nucleophilic attack of amine groups of β-LG to carbonyl groups of PDA, leading to covalent bond formation [66]. Shifting the peak around 1600 cm^{-1} and changing its intensity as a function of β-LG concentration may show the formation of the C=N bond through the Schiff base reaction. Additionally, amide, hydroxyl, and carboxyl functional groups of β-LG can undergo hydrogen bonding with hydroxyl functional groups in the PDA chemical structure, stabilizing the protein of the surface [67]. Changes in the intensity of amide I and II in β-LG can indicate alterations in the hydrogen bonding due to the interaction with PDA. Moreover, aromatic rings in the PDA have the potential to interact with aromatic residues in β-LG under π–π stacking [68].

3.3. Protein interaction

β-LG (lower concentration) regularly interacts with the PDA surface at the single-state, as shown in Fig. 3(A). In contrast, β-LG (higher concentration) interaction with the PDA surface becomes irregular at the dimer-state (Fig. 3(B)). Thus, the theoretical findings indicate that the single-state exhibits a homogeneous distri-

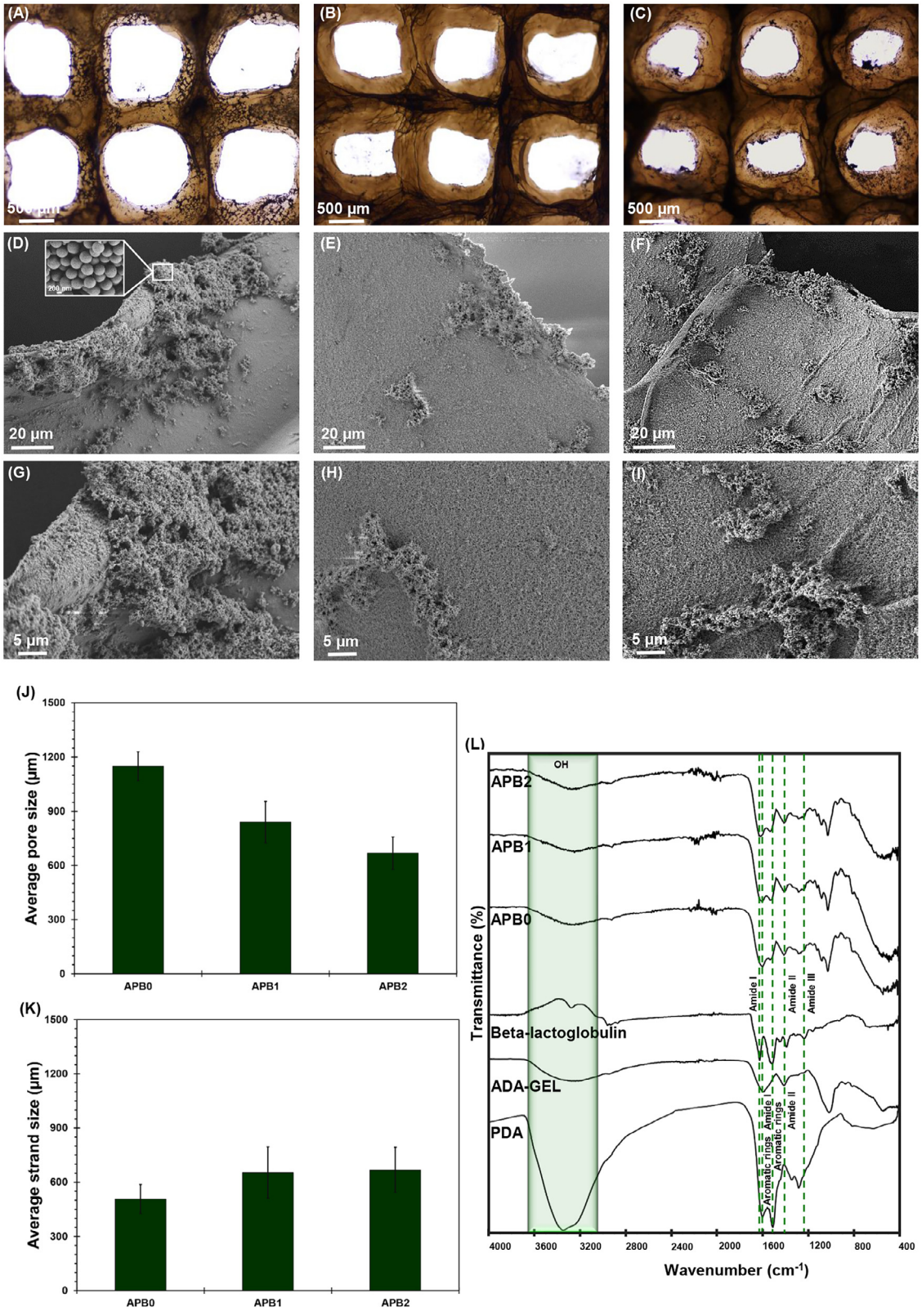

Fig. 2. Microstructural and chemical evaluation of scaffolds. (A–C) optical microscopy images and (D–I) FE-SEM images of (A, D, G) APB0, (B, E, H) APB1, and (C, F, I) APB2 scaffolds. (J) Average pore diameter and (K) average strand thickness of scaffolds. (L) Chemical characterization of polymeric scaffolds. FTIR spectra of PDA, ADA-GEL, β-LG and APB0, APB1, and APB2 scaffolds.

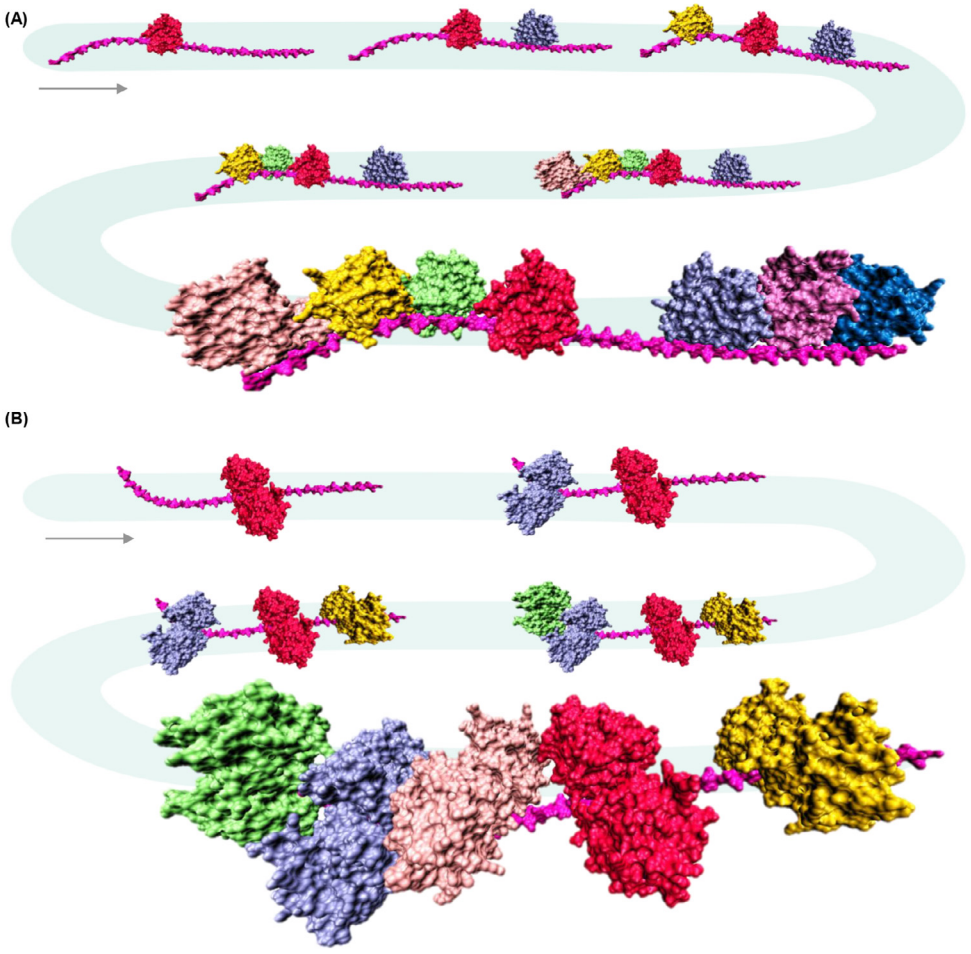

Fig. 3. Molecular docking calculations of β-LG interaction with PDA surface. (A) Single β-LG interaction with the PDA surface, representing the impact of low concentration. (B) β-LG dimer-state interaction with the PDA surface, representing the impact of high concentration.

bution in comparison with the dimer-state on the PDA surface. Accordingly, theoretical findings suggest that β-LG concentration affects the way in which the protein layer forms on the surface. Furthermore, the final theoretical binding energy calculated for the dimer-surface complex (−530.48 kcal/mol) is significantly higher than that calculated for the single-state surface complex (−191.20 kcal/mol). The findings indicate that the interaction between the protein and the surface occurs spontaneously in both the dimeric- and single-state. However, the dimer structure has a higher affinity to interact with surface compared to the single-state. In addition, findings indicate that the process occurs spontaneously in both states, although the dimer structure exhibits the phenomenon more prominently. Moreover, the calculated binding energy indicates an uncontrollable interaction between the surface and the dimer structure as opposed to a controlled interaction between the surface and the single-state. In other words, the low concentration exhibits favourable structural compatibility with the PDA-coated surface. This suggests that the PDA layer on the scaffold adapts structurally to accommodate the uniform growth of a layer of β-LG on the PDA surface, indicating improved biocompatibility of the scaffold. The presence of a well-structured β-LG layer on the surface can enhance cell adhesion, proliferation, and functionality, contributing to improved tissue integration and regeneration [69]. These findings are based on computational simulations; hence, we carried out further studies to evaluate how single- and dimer-state surface complex influence effectiveness of scaffolds for subchondral bone regeneration.

3.4. Absorption capacity and degradation

Evaluating the absorption capacity of scaffolds is necessary, as it determines scaffolds' potential for nutrient transport, the release of signalling molecules, cell adhesion, and tissue regeneration. In this study, we investigated the absorption capacity of multi-material and multi-layered scaffolds over time, as shown in Fig. 4(A). Obtained results demonstrated the impressive ability of scaffolds to absorb fluids, indicating the suitability of constructs for tissue engineering applications. All the experimental groups showed a notable capacity for absorption of fluids during the initial 2 h, arising from hydrophilic functional groups in the chemical composition of scaffolds and the interconnected porous structure of scaffolds, enabling easy fluid transfer. Over time, the absorption increased gradually, reaching equilibrium swelling after 96 h. Equilibrium absorption ratios of APB0 were 5481 ± 957 % after 96 h. However, coating the scaffolds with β-LG increased this value to 6772 ± 241 and 7686 ± 249 % for APB1 and APB2, respectively, after 96 h of incubation, suggesting β-LG increased the scaffold's ability to absorb fluids compared to the uncoated scaffolds. Additionally, increasing the concentration of protein showed significant enhancement in absorption capacity. Herein, β-LG possesses hydrophilic properties due to polar amino acid residues, facilitating the penetration of the fluid into the scaffold. Furthermore, β-LG can introduce abundant hydroxyl and amine functional groups, which can engage in hydrogen bonding with water molecules, contributing to a greater uptake of fluids. The improved absorption ratio achieved through

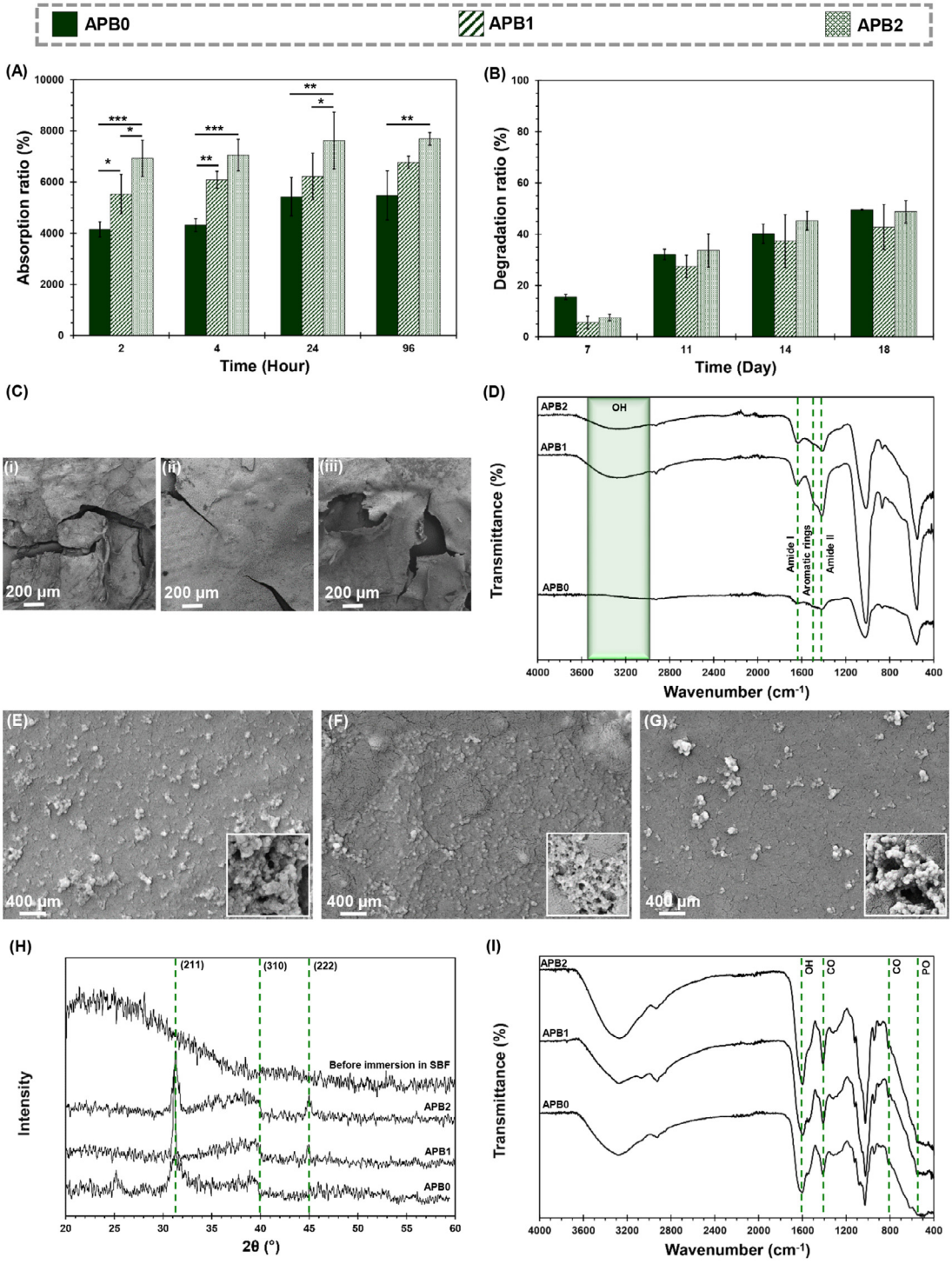

Fig. 4. Interaction of scaffolds with biological-like fluids. (A) Absorption ratio of APB0, APB1, APB2 scaffolds over time (2, 4, 24 and 96 h). (B) Degradation ratio of APB0, APB1, APB2 scaffolds over time (7, 11, 14 and 18 days). Differences are considered statistically significant ($^{*}P \leq 0.05$; $^{**}P < 0.01$; $^{***}P < 0.001$). (C) FE-SEM images of (i) APB0 and (ii) APB1, and (iii) APB2 scaffolds and (D) FTIR spectra of degraded scaffolds after 18 days of immersion in cell culture medium. (E-I) *In-vitro* bioactivity of the scaffolds. (E-G) FE-SEM images of (E) APB0 and (F) APB1, and (G) APB2 scaffolds after 18 days of immersion in the SBF solution. (H) FTIR spectra and (I) XRD pattern of scaffolds after biomineralization of HA-like layers.

β-LG coating highlights the potential to tailor the properties of scaffolds to meet tissue regeneration.

Degradation tests evaluate the scaffold's biocompatibility, degradation rate, and suitability for supporting tissue regeneration and integration in the body. The chemical composition of scaffolds along with the fabrication methods has a significant impact on both the degradation process and the biocompatibility. Therefore, it is crucial to have a comprehensive understanding of the degradation behaviour of scaffolds, which is essential for designing scaffolds with optimal degradation profile and minimizing harmful by-products [70]. Fig. 4(B) illustrates the degradation ratio relative to hydrogel weight. It was noted that the 18-day degradation ratio was 50 $\pm$ 0.2, 43 $\pm$ 9, and 49 $\pm$ 4 % for APB0, APB1, and APB2 scaffolds, respectively. Stable increase in the degradation ratio was observed during 18 days of incubation. While APB0 scaffolds exhibited higher degradation values compared to the other groups, and ABP1 scaffolds with lower concentrations of β-LG demonstrated lower degradation values than APB2, it is important to note that statistical evaluation revealed no significant differences between the experimental groups in terms of degradation. While a significant increase was observed in the absorption capacity of β-LG coated scaffolds compared with uncoated scaffolds, there was no significant increase in the degradation rate, which may arise from the role of β-LG, leading to the formation of a stable coating layer, acting as a protective barrier, and preserving the structural integrity of coated scaffolds. In this condition, the coating layer may provide mechanical support to the scaffold [71], preventing the scaffolds from undergoing physical changes or disintegration. Also, a lower concentration of β-LG with ordered deposition of β-LG, as suggested in docking calculations, reduces the scaffolds' hydrophilicity, which decreases the absorption ratio and controls degradation. These findings emphasize the crucial role of the β-LG coating in maintaining scaffold stability and controlling degradation.

The FE-SEM images after 18 days of degradation test Fig. 4(C) were along with the results of the degradation ratio and indicated crack formation in printed strands after the immersion of samples in cell-culture medium. Interestingly, β-LG-containing scaffolds (APB1 and APB2) exhibited higher stability and lower crack formation compared to the uncoated samples. Furthermore, it was observed that the lower concentration of β-LG provided the highest stability. This suggests that the protein coating and its ordered deposition played a crucial role in improving the overall structural integrity of the scaffolds.

In addition to the FE-SEM analysis, FTIR spectroscopy was performed to further investigate the structural changes that occurred during the degradation of scaffolds. Specifically, the intensities of the amide I ($\sim$ 1600 cm^{-1}), amide II ($\sim$ 1400–1600 cm^{-1}), aromatic rings ($\sim$ 1500–1600 cm^{-1}), and hydroxyl ($\sim$ 3000–3500 cm^{-1}) functional groups were reduced following 18 days immersion of scaffolds in cell culture medium, indicating changes in the molecular composition of the scaffolds upon degradation especially in uncoated scaffolds (APB0). In β-LG-containing scaffolds, lower protein concentration demonstrated less reduction in peak intensities, suggesting a protective effect against degradation and preserving the structural integrity. The reduction in the peaks intensity of the amide I and amide II bonds and aromatic rings can be attributed to the cleavage of amide bonds or peptide bonds in ADA-GEL and protein chains as well as removal of catechol and quinone groups in PDA, breaking the polymer chains into smaller fragments.

3.5. Bioactivity

The development of a hydroxyapatite (HA)-like layer on the surface of scaffolds upon interaction with physiological fluids is recognized as a key characteristic indicating bioactivity in bone regeneration. The precipitation of a dense and uniform mineralized layer is highly advantageous for bone regeneration. HA-like layers not only can improve the biological interaction between the scaffold and osteoblasts but also the formation of this mineralized layer contributes to the osteointegration as well as providing mechanical stability [72]. The FE-SEM images in Fig. 4(E–G) confirm the precipitation of mineralized layers on the scaffolds. The APB0 scaffolds exhibit a locally aggregated calcium phosphate layer, while the β-LG coated scaffolds show a more uniform distribution of the deposited mineral layer after incubation in the SBF solution. The more irregular crystal formation observed on the surface of the APB0 scaffolds suggests a less controlled mineralization process compared to the β-LG-coated ones. This observation can be attributed to the effect of β-LG and its surface chemistry on the nucleation and growth of the mineralized layer. The deposition of a more homogeneous calcium phosphate layer on the scaffolds with a lower concentration of β-LG (APB1) is an interesting finding, which may positively affect scaffold-osteoblasts interactions and improve osteointegration. The ordered deposition of β-LG on the scaffold surface (see docking findings) provides a structured arrangement of molecules, acting as a nucleation site for the accelerated deposition of minerals. Also, the ordered template of β-LG is expected to influence the alignment of mineral deposition, leading to more organized mineral structures with higher similarity to native bone. Also, ordered deposition of β-LG can regulate the biomineralization kinetics [73]. By organizing the arrangement of β-LG, the availability of binding sites for calcium and phosphate ions can be controlled, influencing the rate of calcium-phosphate deposition.

The XRD analysis (Fig. 4(H)) confirms the formation of HA on scaffolds, which is proven by specific peaks at 2θ angles of 31.84º, 39.65º, and 44.98º are assigned to crystallographic planes (211), (310), and (222), respectively [74,75]. The presence of these distinct peaks confirms the successful formation of pure HA crystals, resembling the composition of natural bone. Fig. 4(I) shows the FTIR spectra after bioactivity analysis. A characteristic peak at 553 cm^{-1} is related to the P–O bonds. Also, O-H stretching vibration was identified by a peak at 1603 cm^{-1}. Additionally, C–O vibrations, observed at 813 cm^{-1} and 1420 cm^{-1}, are indicators of carbonated-HA formation [76], resembling the composition of physiological HA. Carbonate hydroxyapatite formation is possible when calcium and magnesium ions are present in the media. As a consequence, magnesium ions in solution have a higher degree of hydration than calcium ions, resulting in a higher concentration of hydrated magnesium ions in the solution, which may result in the deposition of carbonate hydroxyapatite that closely mimics physiological HA, enhancing bioactivity and bioresorbable [77]. The FTIR spectra and XRD pattern indicate that β-LG coating on the scaffolds increases the intensity of peaks belonging to mineralized HA. One possible explanation for this finding is that β-LG acts as a stabilizing agent for HA formation, inhibiting the breakdown of HA, preventing its dissolution, promoting the growth of HA crystals, and maintaining its structural integrity. Daskalakis et al. [78] also demonstrated that β-LG reduces the dissolution of grown HA layers. Also, the amine and hydroxyl functional groups in the chemical structure of β-LG may trigger the nucleation sites for mineralization [79]. According to obtained results, a lower concentration of β-LG (APB1) shows the highest peak intensity, which aligns with the FE-SEM observations. The ordered deposition of β-LG at lower concentrations promotes the formation of well-aligned protein layers on the scaffolds, providing suitable binding sites and facilitating the nucleation and growth of HA crystals during the mineralization process.

When scaffolds are immersed in a simulated body fluid solution, the hydroxyl groups within the scaffold release hydrogen

ions, resulting in the deposition of acidic compounds like hydrogen carbonate and hydrogen phosphate onto the scaffold surface. These acidic compounds play a crucial role in promoting the formation of calcium phosphate layers [64]. The scaffold undergoes an initial formation of a thin layer of amorphous calcium phosphate, followed by subsequent interactions between ions and the scaffold surface that result in the development of a crystalline HA layer. These processes are believed to be influenced by charge repulsion and the presence of multiple catecholamines within the PDA chemical structure [80,81]. Also, whey protein isolate (WPI) hydrogels rich in β-LG can enhance and accelerate the formation of mineralized layers [28]. The inherent hydrophilicity of polymers and proteins plays a significant role in facilitating the absorption of calcium and phosphate ions from the SBF solution [76] and facilitate mineralization.

3.6. Cell-scaffold interactions

This study delved into the intricate interplay between cells and scaffolds, specifically focusing on cultivating bone marrow mesenchymal stem cells and human osteoblasts and their interaction with the scaffolds. Cell staining with calcein AM at distinct time points of 2 and 7 days of culture (Fig. 5(A)) affirms the scaffolds' profound capacity to serve as anchorage sites for cells, augmented by the strategic application of β-LG coating. Notably, after 2 days of cultivation, discernible clusters of viable cells were observed, with their robustness and homogeneity further augmented after 7 days, corroborating the progressive maturation and adherence of cells to the scaffolds' microenvironment. Surprisingly, the samples coated with a lower concentration of β-LG exhibited a higher density of viable cells. The ordered deposition of the β-LG at lower concentration provides a more structured, uniform, stable, and well-defined substrate, affecting cell signalling, cell attachment, and spreading, that provides specific binding sites for cell receptors or integrins and allows the cells to establish strong interactions with the scaffold surface, as observed in previous literatures [23]. Additionally, the ordered deposition of β-LG affects the overall stability and integrity of the scaffold surface, which can contribute to maintaining a favourable microenvironment for cell viability.

The viability and proliferation assay (Fig. 5(B)) indicated that cells started to proliferate after two days of incubation. Although the number of viable cells was initially lower than in the control group, the number of viable cells significantly increased with incubation until day 7 in all experimental groups. While the initial observation of reduced viability at the 2-day time point warrants attention, the significant increase in viability over time indicates a dynamic cellular response and suggests that the developed scaffold materials and structure may not exert significant toxic effects on cells, and they may indeed support cell proliferation and functionality over extended culture periods. The proliferation assays demonstrated that β-LG-coated scaffolds exhibited higher cell proliferation compared to non-coated scaffolds. However, it is noteworthy that only the ordered coating demonstrated a significant increase in cell viability compared to the APB0 group after 7 days. The lack of significance between the APB1 and APB2 groups may stem from the initial cellular recognition of the protein, which may not initially consider the architectural differences. Subsequently, cells may begin to respond to physical cues or protein conformation changes, leading to variations in cell behaviour, as observed in cell differentiation studies with longer period. Significant increment in viability of the cells on APB1 scaffolds compared with APB0 may arise from ordered protein architectures facilitate more straightforward protein conformational changes, whereas irregular architectures may impede such changes [82], thus influencing cellular adhesion and proliferation. The other possible reason can be attributed to adjusting surface energy by ordered architecture of protein on the surface and enhancing cell receptor interaction sites. In an investigation, it was demonstrated that the process of protein conformational changes is profoundly influenced by the underlying surface energy, consequently exerting a significant impact on cellular adhesion [83]. Accordingly, it is expected that the ordered deposition of β-LG on the scaffold to be able to create a more organized surface topography, providing physical cues for attachment of cells and facilitating cell adhesion and proliferation [23].

ALP is a well-established non-collagenous biomarker for osteogenesis, and its activity increases early in osteogenesis, even before the expression of other genes associated with mature osteoblasts [84–86]. The enzymatic activity of ALP was meticulously assessed at the 14-day and 21-day time points following cellular culture (Fig. 5(C)). All experimental groups demonstrated notable enhancements in ALP secretion after 21 days. Notably, scaffolds adorned with a coating of 1 mg/ml β-LG exhibited a remarkable up-regulation in ALP levels, suggestive of their exceptional potential in stimulating osteogenic activity. In line with our findings, another study demonstrated dose-dependent ALP production when osteoblasts were cultured on whey protein isolate [87]. Immunocytochemistry (Fig. 5(D)) analysis investigated the impact of β-LG coatings on osteogenic differentiation by determining the expression of SPP1 and COL1A1 through immunofluorescence staining after 21 days of human osteoblast culture. By using human osteoblasts, which are more closely related to the human system, we tried to increase the biological relevance and translational potential of our findings. The results demonstrated that scaffolds containing β-LG coatings exhibited evident expression of SPP1 and COL1A1, which are key markers associated with osteoblast differentiation. SPP1, a multifunctional protein, participates in the regulation of mineralization [88], and COL1A1, the predominant protein in bone matrix, provides structural integrity, facilitates mineralization, and regulates cell signalling [89]. This finding suggests that the presence of β-LG promotes the expression of genes related to osteogenesis. In contrast, APB0 scaffolds displayed lower expression levels of SPP1 and COL1A1, indicating lower osteogenic differentiation potential. Interestingly, the group with a lower concentration of β-LG (APB1) exhibited an up-regulation of SPP1 and COL1A1 compared to APB2 scaffolds. This phenomenon can be attributed to the ordered deposition of proteins on the scaffold surface in lower β-LG concentrations, creating a more structured and uniform environment, which may enhance the signalling pathways involved in osteogenic differentiation.

These compelling observations serve to emphasize the extraordinary prowess of the PDA-functionalized surface, wherein its remarkable ability to proficiently absorb bioactive molecules imparts a multifaceted role in fostering cellular differentiation and bone regeneration [90]. PDA has shown anti-inflammatory and antioxidative effects, creating an environment conducive to osteoblast function and differentiation [91]. Besides, β-LG coatings can potentially enhance cell adhesion, proliferation, and osteogenic differentiation. As a carrier protein, β-LG facilitates the delivery of bioactive molecules that promote osteogenesis, improving their solubility and bioavailability. Furthermore, β-LG has an affinity for hydrophobic molecules that promote osteogenic differentiation and can interact with signalling pathways involved in osteoblast function and bone regeneration [69]. The synergistic cooperation between PDA and β-LG enhances cell-material interactions, stabilizes the surface, and facilitates the delivery of bioactive molecules, supporting cell attachment, proliferation, and osteogenic gene expression. More studies could further explore the underlying mechanisms behind the effects of β-LG coatings on osteogenic differentiation, including signalling pathways and the specific interactions between the ordered protein layer and osteoblasts that would pro-

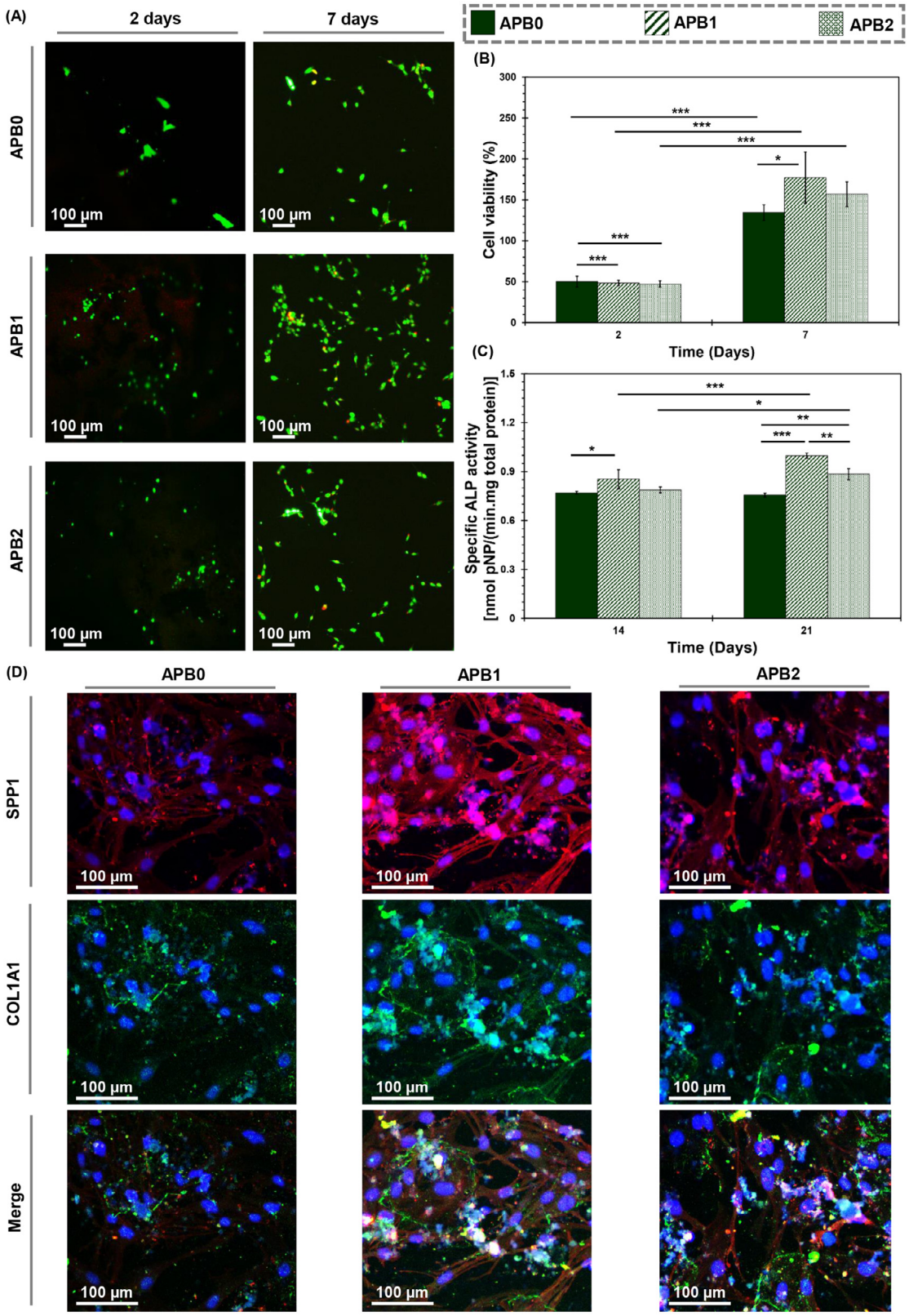

Fig. 5. Cell-scaffolds interactions. (A) Bone marrow mesenchymal stem cells staining with calcein-AM and propidium iodide after 2 and 7 days culture on APB0, APB1, and APB2 scaffolds indicating cell viability. (B) Proliferation of bone marrow mesenchymal stem cells on the scaffolds as a function of incubation time. (C) ALP activity of bone marrow mesenchymal stem cells on the scaffolds after 14 and 21 days of culture. Differences are considered statistically significant ($^{*}P \leq 0.05$; $^{**}P < 0.01$; $^{***}P < 0.001$). (D) Osteogenic differentiation of human osteoblasts. Immunofluorescence staining of SPP1 and COL1A1 in human osteoblast after 21 days culture on APB0, APB1, and APB2 scaffolds.

vide valuable insights for translational applications in regenerative medicine.

4. Conclusion

In this study, 3D printed ADA-GEL scaffolds were meticulously engineered to harness their innate potential for promoting subchondral bone regeneration. To amplify their regenerative capabilities, a bioinspired approach was employed, involving the application of a PDA coating, inspired by adhesive proteins derived from mussels. Additionally, a tailored multi-layered scaffold design was implemented, where the bi-layered scaffolds were subsequently coated with two distinct concentrations (1 mg/ml and 2 mg/ml) of β-LG, aiming to achieve synergistic effects that enhance osteogenic potential. In addition to morphological and physicochemical evaluations, this study also encompassed protein interaction simulations and rigorous *in-vitro* performance assessments. The outcomes of these comprehensive analyses demonstrated the successful fabrication of tubular-like pores through the utilization of advanced 3D printing technology. This innovative approach enables crucial functionalities such as efficient nutrient supply, vital ion exchange, and stimulation of cellular growth, thus establishing a favourable environment for cellular activities. The coating of β-LG on the scaffolds improved the absorption capacity and controlled the degradation process, with the lower concentration of β-LG providing a durable structure. In addition, β-LG and PDA synergistically promoted the biomimetic formation of HA layers. Unlike the single-state, protein interaction simulations showed that the dimer-state has a greater affinity for interacting with the surface of PDA. Molecular docking calculations indicated uncontrolled interactions between the PDA surface and the dimer structure, while controlled interactions were observed between the single β-LG molecule and the PDA surface. Coating the scaffolds facilitated the adhesion and proliferation of bone marrow mesenchymal stem cells. Osteodifferentiation was demonstrated by increased ALP activity and expression of SPP1 and COL1A1, particularly after surface treatment with the lower concentration of β-LG (1 mg/ml). Overall, the developed multi-layered scaffolds demonstrated promising potential as advanced biomaterials for subchondral bone tissue engineering applications. While our scaffold size and shape serve as a base model, it is crucial to highlight the customization potential and patient-specific design capabilities enabled by 3D printing. Looking ahead, defect geometry data from MRI or CT scans can inform personalized scaffold designs using this advanced fabrication technique for clinical applications.

Declaration of competing interest

The authors whose names are listed certify that they have NO affiliations with or involvement in any organization or entity with any financial interest (such as honoraria; educational grants; participation in speakers' bureaus; membership, employment, consultancies, stock ownership, or other equity interest; and expert testimony or patent-licensing arrangements), or non-financial interest (such as personal or professional relationships, affiliations, knowledge or beliefs) in the subject matter or materials discussed in this manuscript.

CRediT authorship contribution statement

Farnaz Ghorbani: Conceptualization, Data curation, Funding acquisition, Investigation, Methodology, Validation, Visualization, Writing – original draft, Writing – review & editing. **Minjoo Kim:** Investigation, Methodology. **Behafarid Ghalandari:** Conceptualization, Investigation, Methodology, Writing – original draft. **Mingjing Zhang:** Investigation, Methodology. **Swastina Nath Varma:** Investigation, Methodology. **Lisa Schöbel:** Investigation, Methodology. **Chaozong Liu:** Conceptualization, Funding acquisition, Project administration, Supervision, Writing – review & editing. **Aldo R. Boccaccini:** Conceptualization, Funding acquisition, Project administration, Supervision, Writing – review & editing.

Acknowledgment

This work was supported by the Bavarian Funding Programme for the Initiation of International Projects (Bayerische Forschungs Allianz, project Nr. BayIntAn_FAU_2022_85) and the Alexander von Humboldt Foundation (fellowship to FG).

Data availability

The data supporting this study's findings are available from the corresponding author upon reasonable request.

References

[1] D. Chen, Osteoarthritis: a complicated joint disease requiring extensive studies with multiple approaches, J. Orthop. Transl. 32 (2022) 130, doi:10.1016/j.jot.2022.02.009.
[2] P. Morouço, C. Fernandes, W. Lattanzi, Challenges and innovations in osteochondral regeneration: insights from biology and inputs from bioengineering toward the optimization of tissue engineering strategies, J. Funct. Biomater. 12 (2021) 17, doi:10.3390/jfb12010017.
[3] A. Chmielewska, D. Dean, The role of stiffness-matching in avoiding stress shielding-induced bone loss and stress concentration-induced skeletal reconstruction device failure, Acta Biomater. 173 (2024) 51–65, doi:10.1016/j.actbio.2023.11.011.
[4] R. Marsell, T.A. Einhorn, The biology of fracture healing, Injury 42 (2011) 551–555, doi:10.1016/j.injury.2011.03.031.
[5] T. Yang, M. Tamaddon, L. Jiang, J. Wang, Z. Liu, Z. Liu, H. Meng, Y. Hu, J. Gao, X. Yang, Y. Zhao, Y. Wang, A. Wang, Q. Wu, C. Liu, J. Peng, X. Sun, Q. Xue, Bilayered scaffold with 3D printed stiff subchondral bony compartment to provide constant mechanical support for long-term cartilage regeneration, J. Orthop. Transl. 30 (2021) 112–121, doi:10.1016/j.jot.2021.09.001.
[6] J.J. Wood, Autologous cultured chondrocytes: adverse events reported to the united states food and drug administration, J. Bone Jt. Surg. 88 (2006) 503, doi:10.2106/JBJS.E.00103.
[7] S. Grässel, J. Lorenz, Tissue-engineering strategies to repair chondral and osteochondral tissue in osteoarthritis: use of mesenchymal stem cells, Curr. Rheumatol. Rep. 16 (2014) 452, doi:10.1007/s11926-014-0452-5.
[8] D. Schaefer, I. Martin, P. Shastri, R.. Padera, R. Langer, L. Freed, G. Vunjak-Novakovic, In vitro generation of osteochondral composites, Biomaterials 21 (2000) 2599–2606, doi:10.1016/S0142-9612(00)00127-7.
[9] M. Mirkhalaf, Y. Men, R. Wang, Y. No, H. Zreiqat, Personalized 3D printed bone scaffolds: a review, Acta Biomater. 156 (2023) 110–124, doi:10.1016/j.actbio.2022.04.014.
[10] A. Serafin, M. Culebras, J.M. Oliveira, J. Koffler, M.N. Collins, 3D printable electroconductive gelatin-hyaluronic acid materials containing polypyrrole nanoparticles for electroactive tissue engineering, Adv. Compos. Hybrid Mater. 6 (2023) 109. https://doi.org/10.1007/s42114-023-00665-w.
[11] F. Ghorbani, B. Ghalandari, M. Khajehmohammadi, N. Bakhtiary, H. Tolabi, M. Sahranavard, S. Fathi-Karkan, V. Nazar, S. Hasan Niari Niar, A. Armoon, M. Ettelaei, M. Tavakoli Banizi, M.N. Collins, Photo-cross-linkable hyaluronic acid bioinks for bone and cartilage tissue engineering applications, Int. Mater. Rev. 68 (2023) 901–942, doi:10.1080/09506608.2023.2167559.
[12] W. Ding, Y. Wang, J. Sun, L. Bao, X. Pang, Dialdehyde sodium alginate bonded dicyandiamide for formaldehyde-free leather production with enhanced properties, Carbohydr. Polym. 295 (2022) 119838, doi:10.1016/j.carbpol.2022.119838.
[13] K. Varaprasad, C. Karthikeyan, M.M. Yallapu, R. Sadiku, The significance of biomacromolecule alginate for the 3D printing of hydrogels for biomedical applications, Int. J. Biol. Macromol. 212 (2022) 561–578, doi:10.1016/j.ijbiomac.2022.05.157.
[14] M. Ghanbari, A. Sadjadinia, N. Zahmatkesh, F. Mohandes, B. Dolatyar, B. Zeynali, M. Salavati-Niasari, Synthesis and investigation of physicochemical properties of alginate dialdehyde/gelatin/ZnO nanocomposites as injectable hydrogels, Polym. Test. 110 (2022) 107562, doi:10.1016/j.polymertesting.2022.107562.
[15] A. Serafin, M. Culebras, M.N. Collins, Synthesis and evaluation of alginate, gelatin, and hyaluronic acid hybrid hydrogels for tissue engineering applications, Int. J. Biol. Macromol. 233 (2023) 123438, doi:10.1016/j.ijbiomac.2023.123438.
[16] N. Di Caprio, J.A. Burdick, Engineered biomaterials to guide spheroid formation, function, and fabrication into 3D tissue constructs, Acta Biomater. 165 (2023) 4–18, doi:10.1016/j.actbio.2022.09.052.

[17] A. Hassouna, H. Elgharbawy, R. Morsy, Development of porous scaffolds based on the in situ synthesis of biphasic calcium phosphate in a gelatin-polyvinyl alcohol matrix for bone tissue engineering, J. Mol. Struct. 1279 (2023) 134951, doi:10.1016/j.molstruc.2023.134951.
[18] S. Heid, A.R. Boccaccini, Advancing bioinks for 3D bioprinting using reactive fillers: a review, Acta Biomater. 113 (2020) 1–22, doi:10.1016/j.actbio.2020.06.040.
[19] A. Kostenko, S. Swioklo, C.J. Connon, Alginate in corneal tissue engineering, Biomed. Mater. 17 (2022) 022004, doi:10.1088/1748-605X/ac4d7b.
[20] Y. Tang, Y. Tan, K. Lin, M. Zhu, Research progress on polydopamine nanoparticles for tissue engineering, Front. Chem. 9 (2021) 727123, doi:10.3389/fchem.2021.727123.
[21] P. Feng, M. Liu, S. Peng, S. Bin, Z. Zhao, C. Shuai, Polydopamine modified polycaprolactone powder for fabrication bone scaffold owing intrinsic bioactivity, J. Mater. Res. Technol. 15 (2021) 3375–3385, doi:10.1016/j.jmrt.2021.09.137.
[22] Y. Yu, X. Li, J. Li, D. Li, Q. Wang, W. Teng, Dopamine-assisted co-deposition of hydroxyapatite-functionalised nanoparticles of polydopamine on implant surfaces to promote osteogenesis in environments with high ROS levels, Mater. Sci. Eng. C 131 (2021) 112473, doi:10.1016/j.msec.2021.112473.
[23] B. Ghalandari, Y. Yu, F. Ghorbani, A.R. Warden, K.Z. Ahmad, X. Sang, S. Huang, Y. Zhang, W. Su, A. Divsalar, X. Ding, Polydopamine nanospheres coated with bovine serum albumin permit enhanced cell differentiation: fundamental mechanism and practical application for protein coating formation, Nanoscale 13 (2021) 20098–20110, doi:10.1039/D1NR07469E.
[24] M. Sahebalzamani, M. Ziminska, H.O. McCarthy, T.J. Levingstone, N.J. Dunne, A.R. Hamilton, Advancing bone tissue engineering one layer at a time: a layer-by-layer assembly approach to 3D bone scaffold materials, Biomater. Sci. 10 (2022) 2734–2758, doi:10.1039/D1BM01756J.
[25] M. Szpalski, R. Gunzburg, Recombinant human bone morphogenetic protein-2: a novel osteoinductive alternative to autogenous bone graft? Acta Orthop. Belg. 71 (2005) 133–148 http://www.ncbi.nlm.nih.gov/pubmed/16152845.
[26] C.E. Gillman, A.C. Jayasuriya, FDA-approved bone grafts and bone graft substitute devices in bone regeneration, Mater. Sci. Eng. C 130 (2021) 112466, doi:10.1016/j.msec.2021.112466.
[27] T.E.L. Douglas, M. Vandrovcová, N. Kročilová, J.K. Keppler, J. Zárubová, A.G. Skirtach, L. Bačáková, Application of whey protein isolate in bone regeneration: effects on growth and osteogenic differentiation of bone-forming cells, J. Dairy Sci. 101 (2018) 28–36, doi:10.3168/jds.2017-13119.
[28] K. Norris, M. Kocot, A.M. Tryba, F. Chai, A. Talari, L. Ashton, B.V. Parakhonskiy, S.K. Samal, N. Blanchemain, E.E. Pamuła, T.E.L.L. Douglas, Marine-inspired enzymatic mineralization of dairy-derived whey protein isolate (WPI) hydrogels for bone tissue regeneration, Mar. Drugs 18 (2020) 294, doi:10.3390/md18060294.
[29] D. Gupta, M. Kocot, A.M. Tryba, A. Serafim, I.C. Stancu, Z. Jaegermann, E. Pamuła, G.C. Reilly, T.E.L. Douglas, Novel naturally derived whey protein isolate and aragonite biocomposite hydrogels have potential for bone regeneration, Mater. Des. 188 (2020) 108408, doi:10.1016/j.matdes.2019.108408.
[30] F. Ghorbani, M. Kim, M. Monavari, B. Ghalandari, A.R. Boccaccini, Mussel-inspired polydopamine decorated alginate dialdehyde-gelatin 3D printed scaffolds for bone tissue engineering application, Front. Bioeng. Biotechnol. 10 (2022), doi:10.3389/fbioe.2022.940070.
[31] J.M. Oliveira, V.P. Ribeiro, R.L. Reis, Advances on gradient scaffolds for osteochondral tissue engineering, Prog. Biomed. Eng. 3 (2021) 033001, doi:10.1088/2516-1091/abfc2c.
[32] B. Sarker, D.G. Papageorgiou, R. Silva, T. Zehnder, F. Gul-E-Noor, M. Bertmer, J. Kaschta, K. Chrissafis, R. Detsch, A.R. Boccaccini, Fabrication of alginate–gelatin crosslinked hydrogel microcapsules and evaluation of the microstructure and physico-chemical properties, J. Mater. Chem. B 2 (2014) 1470, doi:10.1039/c3tb21509a.
[33] B. Sarker, J. Rompf, R. Silva, N. Lang, R. Detsch, J. Kaschta, B. Fabry, A.R. Boccaccini, Alginate-based hydrogels with improved adhesive properties for cell encapsulation, Int. J. Biol. Macromol. 78 (2015) 72–78, doi:10.1016/j.ijbiomac.2015.03.061.
[34] B. Sarker, R. Singh, R. Silva, J.A. Roether, J. Kaschta, R. Detsch, D.W. Schubert, I. Cicha, A.R. Boccaccini, Evaluation of fibroblasts adhesion and proliferation on alginate-gelatin crosslinked hydrogel, PLoS One 9 (2014) e107952, doi:10.1371/journal.pone.0107952.
[35] M.M. Monavari, S. Homaeigohar, M. Fuentes-Chandía, Q. Nawaz, M.M. Monavari, A. Venkatraman, A.R. Boccaccini, 3D printing of alginate dialdehyde-gelatin (ADA-GEL) hydrogels incorporating phytotherapeutic icariin loaded mesoporous SiO_2-CaO nanoparticles for bone tissue engineering, Mater. Sci. Eng. C 131 (2021) 112470, doi:10.1016/j.msec.2021.112470.
[36] T. Kreller, T. Distler, S. Heid, S. Gerth, R. Detsch, A.R. Boccaccini, Physico-chemical modification of gelatine for the improvement of 3D printability of oxidized alginate-gelatine hydrogels towards cartilage tissue engineering, Mater. Des. 208 (2021) 109877, doi:10.1016/J.MATDES.2021.109877.
[37] S. Heid, K. Becker, J. Byun, I. Biermann, Z. Neščáková, H. Zhu, J. Groll, A.R. Boccaccini, Bioprinting with bioactive alginate dialdehyde-gelatin (ADA-GEL) composite bioinks: Time-dependent in-situ crosslinking via addition of calcium-silicate particles tunes in vitro stability of 3D bioprinted constructs, Bioprinting 26 (2022) e00200, doi:10.1016/j.bprint.2022.e00200.
[38] T. Distler, C. Polley, F. Shi, D. Schneidereit, M.D. Ashton, O. Friedrich, J.F. Kolb, J.G. Hardy, R. Detsch, H. Seitz, A.R. Boccaccini, Electrically conductive and 3D-printable oxidized alginate-gelatin polypyrrole:PSS hydrogels for tissue engineering, Adv. Healthc. Mater. 10 (2021). https://doi.org/10.1002/adhm.202001876.
[39] Y.D. Nokoorani, A. Shamloo, M. Bahadoran, H. Moravvej, Fabrication and characterization of scaffolds containing different amounts of allantoin for skin tissue engineering, Sci. Rep. 11 (2021) 16164, doi:10.1038/s41598-021-95763-4.
[40] A. Montes, D. Valor, L. Delgado, C. Pereyra, E. Martínez de la Ossa, An attempt to optimize supercritical CO_2 polyaniline-polycaprolactone foaming processes to produce tissue engineering scaffolds, Polymers (Basel) 14 (2022) 488, doi:10.3390/polym14030488.
[41] J. Loch, A. Polit, A. Górecki, P. Bonarek, K. Kurpiewska, M. Dziedzicka-Wasylewska, K. Lewiński, Two modes of fatty acid binding to bovine β-lactoglobulin-crystallographic and spectroscopic studies, J. Mol. Recognit. 24 (2011) 341–349, doi:10.1002/jmr.1084.
[42] F. Ghorbani, B. Ghalandari, C. Liu, A facile method to synthesize 3D pomegranate-like polydopamine microspheres, Front. Bioeng. Biotechnol. 9 (2021) 1293, doi:10.3389/fbioe.2021.737074.
[43] J. Yoo, A. Aksimentiev, Improved parameterization of amine–carboxylate and amine–phosphate interactions for molecular dynamics simulations using the CHARMM and AMBER force fields, J. Chem. Theory Comput. 12 (2016) 430–443, doi:10.1021/acs.jctc.5b00967.
[44] D. Mercadante, L.D. Melton, G.E. Norris, T.S. Loo, M.A.K. Williams, R.C.J. Dobson, G.B. Jameson, Bovine β-lactoglobulin is dimeric under imitative physiological conditions: dissociation equilibrium and rate constants over the pH range of 2.5–7.5, Biophys. J. 103 (2012) 303–312, doi:10.1016/j.bpj.2012.05.041.
[45] L. Vijayalakshmi, R. Krishna, R. Sankaranarayanan, M. Vijayan, An asymmetric dimer of β-lactoglobulin in a low humidity crystal form—Structural changes that accompany partial dehydration and protein action, Proteins Struct. Funct. Bioinform. 71 (2008) 241–249, doi:10.1002/prot.21695.
[46] Y. Yan, H. Tao, J. He, S.-Y. Huang, The HDOCK server for integrated protein–protein docking, Nat. Protoc. 15 (2020) 1829–1852, doi:10.1038/s41596-020-0312-x.
[47] Y. Yan, D. Zhang, P. Zhou, B. Li, S.-Y. Huang, HDOCK: a web server for protein–protein and protein–DNA/RNA docking based on a hybrid strategy, Nucleic Acids Res. 45 (2017) W365–W373, doi:10.1093/nar/gkx407.
[48] W. Humphrey, A. Dalke, K. Schulten, VMD: Visual molecular dynamics, J. Mol. Graph. 14 (1996) 33–38, doi:10.1016/0263-7855(96)00018-5.
[49] J.L. Hernandez, K.A. Woodrow, Medical applications of porous biomaterials: features of porosity and tissue-specific implications for biocompatibility, Adv. Healthc. Mater. 11 (2022) 2102087, doi:10.1002/adhm.202102087.
[50] P. Xia, Y. Luo, Vascularization in tissue engineering: The architecture cues of pores in scaffolds, J. Biomed. Mater. Res. Part B Appl. Biomater. 110 (2022) 1206–1214, doi:10.1002/jbm.b.34979.
[51] N.O. Monteiro, J.F. Fangueiro, R.L. Reis, N.M. Neves, Replication of natural surface topographies to generate advanced cell culture substrates, Bioact. Mater. 28 (2023) 337–347, doi:10.1016/j.bioactmat.2023.06.002.
[52] F. Etezadi, M.N.T. Le, H. Shahsavarani, A. Alipour, N. Moazzezy, S. Samani, A. Amanzadeh, S. Pahlavan, S. Bonakdar, M.A. Shokrgozar, K. Hasegawa, Optimization of a PDMS-based cell culture substrate for high-density human-induced pluripotent stem cell adhesion and long-term differentiation into cardiomyocytes under a xeno-free condition, ACS Biomater. Sci. Eng. 8 (2022) 2040–2052, doi:10.1021/acsbiomaterials.2c00162.
[53] X. Pan, Y. Li, A.O. Abdullah, W. Wang, M. Qi, Y. Liu, Micro/nano-hierarchical structured TiO 2 coating on titanium by micro-arc oxidation enhances osteoblast adhesion and differentiation, R. Soc. Open Sci. 6 (2019) 182031, doi:10.1098/rsos.182031.
[54] K. Klimek, G. Ginalska, Proteins and peptides as important modifiers of the polymer scaffolds for tissue engineering applications—a review, Polymers (Basel) 12 (2020) 844, doi:10.3390/polym12040844.
[55] M. Assfalg, Protein adsorption and conformational changes, Molecules 26 (2021) 7079, doi:10.3390/molecules26237079.
[56] Y. Wu, R. Lin, K. Zhang, J. Yan, F. Ma, J. Zhen, J. Pan, Discontinuous cooperative imprinting idea based on MXene-nanocomposite membrane for high structurally stable recognition and separation of shikimic acid, Chem. Eng. J. 460 (2023) 141891, doi:10.1016/j.cej.2023.141891.
[57] C.M. Murphy, F.J. O'Brien, Understanding the effect of mean pore size on cell activity in collagen-glycosaminoglycan scaffolds, Cell Adh. Migr. 4 (2010) 377–381, doi:10.4161/cam.4.3.11747.
[58] N. Abbasi, S. Hamlet, R.M. Love, N.-T. Nguyen, Porous scaffolds for bone regeneration, J. Sci. Adv. Mater. Devices 5 (2020) 1–9, doi:10.1016/j.jsamd.2020.01.007.
[59] P. Deb, A.B. Deoghare, A. Borah, E. Barua, S. Das Lala, Scaffold development using biomaterials: a review, Mater. Today Proc. 5 (2018) 12909–12919, doi:10.1016/j.matpr.2018.02.276.
[60] V. Karageorgiou, D. Kaplan, Porosity of 3D biomaterial scaffolds and osteogenesis, Biomaterials 26 (2005) 5474–5491, doi:10.1016/j.biomaterials.2005.02.002.
[61] M. Dziaduszewska, A. Zieliński, Structural and material determinants influencing the behavior of porous Ti and its alloys made by additive manufacturing techniques for biomedical applications, Materials (Basel) 14 (2021) 712, doi:10.3390/ma14040712.
[62] P. Ouyang, H. Dong, X. He, X. Cai, Y. Wang, J. Li, H. Li, Z. Jin, Hydromechanical mechanism behind the effect of pore size of porous titanium scaffolds on osteoblast response and bone ingrowth, Mater. Des. 183 (2019) 108151, doi:10.1016/j.matdes.2019.108151.
[63] Y. Zhang, N. Sun, M. Zhu, Q. Qiu, P. Zhao, C. Zheng, Q. Bai, Q. Zeng, T. Lu, The contribution of pore size and porosity of 3D printed porous titanium scaffolds to osteogenesis, Mater. Sci. Eng. C (2022) 112651, doi:10.1016/j.msec.2022.112651.

[64] F. Ghorbani, A. Zamanian, A. Behnamghader, M.D. Joupari, A facile method to synthesize mussel-inspired polydopamine nanospheres as an active template for in situ formation of biomimetic hydroxyapatite, Mater. Sci. Eng. C 94 (2019), doi:10.1016/j.msec.2018.10.010.
[65] C. Han, Y. Xiao, E. Liu, Z. Su, X. Meng, B. Liu, Preparation of Ca-alginate-whey protein isolate microcapsules for protection and delivery of L. bulgaricus and L. paracasei, Int. J. Biol. Macromol. 163 (2020) 1361–1368, doi:10.1016/j.ijbiomac.2020.07.247.
[66] J. Yang, M.A. Cohen Stuart, M. Kamperman, Jack of all trades: versatile catechol crosslinking mechanisms, Chem. Soc. Rev. 43 (2014) 8271–8298, doi:10.1039/C4CS00185K.
[67] K.M. Hutchins, Functional materials based on molecules with hydrogen-bonding ability: applications to drug co-crystals and polymer complexes, R. Soc. Open Sci. 5 (2018) 180564, doi:10.1098/rsos.180564.
[68] M. Rahman, Z. Muhseen, M. Junaid, H. Zhang, The aromatic stacking interactions between proteins and their macromolecular ligands, Curr. Protein Pept. Sci. 16 (2015) 502–512, doi:10.2174/1389203716061507021315l6.
[69] M. Rezia Rad, M. Khojaste, M. Hasan Shahriari, S. Asgary, A. Khojasteh, Purmorphamine increased adhesion, proliferation and expression of osteoblast phenotype markers of human dental pulp stem cells cultured on beta-tricalcium phosphate, Biomed. Pharmacother. 82 (2016) 432–438, doi:10.1016/j.biopha.2016.05.016.
[70] A.K. Gaharwar, I. Singh, A. Khademhosseini, Engineered biomaterials for in situ tissue regeneration, Nat. Rev. Mater. 5 (2020) 686–705, doi:10.1038/s41578-020-0209-x.
[71] J.C. Courtenay, C. Deneke, E.M. Lanzoni, C.A. Costa, Y. Bae, J.L. Scott, R.I. Sharma, Modulating cell response on cellulose surfaces; tunable attachment and scaffold mechanics, Cellulose 25 (2018) 925–940, doi:10.1007/s10570-017-1612-3.
[72] Y.-F. Shao, X. Qing, Y. Peng, H. Wang, Z. Shao, K.-Q. Zhang, Enhancement of mechanical and biological performance on hydroxyapatite/silk fibroin scaffolds facilitated by microwave-assisted mineralization strategy, Colloids Surf. B Biointerfaces 197 (2021) 111401, doi:10.1016/j.colsurfb.2020.111401.
[73] X. Deng, A. Hasan, S. Elsharkawy, E. Tejeda-Montes, N.V. Tarakina, G. Greco, E. Nikulina, J.M. Stormonth-Darling, N. Convery, J.C. Rodriguez-Cabello, A. Boyde, N. Gadegaard, N.M. Pugno, M. Al-Jawad, A. Mata, Topographically guided hierarchical mineralization, Mater. Today Bio. 11 (2021) 100119, doi:10.1016/j.mtbio.2021.100119.
[74] F. Ghorbani, B. Ghalandari, A.L. Khan, D. Li, A. Zamanian, B. Yu, Decoration of electrical conductive polyurethane-polyaniline/polyvinyl alcohol matrixes with mussel-inspired polydopamine for bone tissue engineering, Biotechnol. Prog. 36 (2020) e3043, doi:10.1002/btpr.3043.
[75] C. Adler, M. Monavari, G.A. Abraham, A.R. Boccaccini, F. Ghorbani, Mussel-inspired polydopamine decorated silane modified-electroconductive gelatin-PEDOT:PSS scaffolds for bone regeneration, RSC Adv. 13 (2023) 15960–15974, doi:10.1039/D3RA01311A.
[76] F. Ghorbani, A. Zamanian, A. Behnamghader, M. Daliri-Joupari, Bone-like hydroxyapatite mineralization on the bio-inspired PDA nanoparticles using microwave irradiation, Surf. Interfaces. 15 (2019). https://doi.org/10.1016/j.surfin.2019.01.007.
[77] H. Zamin, T. Yabutsuka, S. Takai, H. Sakaguchi, Role of magnesium and the effect of surface roughness on the hydroxyapatite-forming ability of zirconia induced by biomimetic aqueous solution treatment, Materials (Basel) 13 (2020) 3045, doi:10.3390/ma13143045.
[78] K.D. Daskalakis, T.A. Fuierer, J. Tan, G.H. Nancollas, The influence of β-lactoglobulin on the growth and dissolution kinetics of hydroxyapatite, Colloids Surf. A Physicochem. Eng. Asp. 96 (1995) 135–141, doi:10.1016/0927-7757(94)03041-W.
[79] G. Kaynak Bayrak, T.T. Demirtaş, M. Gümüşderelioğlu, Microwave-induced biomimetic approach for hydroxyapatite coatings of chitosan scaffolds, Carbohydr. Polym. 157 (2017) 803–813, doi:10.1016/j.carbpol.2016.10.016.
[80] J. Park, S.J. Lee, T.G. Jung, J.H. Lee, W.D. Kim, J.Y. Lee, S.A. Park, Surface modification of a three-dimensional polycaprolactone scaffold by polydopamine, biomineralization, and BMP-2 immobilization for potential bone tissue applications, Colloids Surf. B Biointerfaces 199 (2021) 111528, doi:10.1016/j.colsurfb.2020.111528.
[81] X. Chen, L. Zhu, H. Liu, W. Wen, H. Li, C. Zhou, B. Luo, Biomineralization guided by polydopamine-modifed poly(L-lactide) fibrous membrane for promoted osteoconductive activity, Biomed. Mater. 14 (2019) 055005, doi:10.1088/1748-605X/AB2F2D.
[82] J.A.O. Rumfeldt, C. Galvagnion, K.A. Vassall, E.M. Meiering, Conformational stability and folding mechanisms of dimeric proteins, Prog. Biophys. Mol. Biol. 98 (2008) 61–84, doi:10.1016/j.pbiomolbio.2008.05.004.
[83] S.H. Ku, J. Ryu, S.K. Hong, H. Lee, C.B. Park, General functionalization route for cell adhesion on non-wetting surfaces, Biomaterials 31 (2010) 2535–2541, doi:10.1016/j.biomaterials.2009.12.020.
[84] E. Castrén, T. Sillat, S. Oja, A. Noro, A. Laitinen, Y.T. Konttinen, P. Lehenkari, M. Hukkanen, M. Korhonen, Osteogenic differentiation of mesenchymal stromal cells in two-dimensional and three-dimensional cultures without animal serum, Stem Cell Res. Ther. 6 (2015) 167, doi:10.1186/s13287-015-0162-6.
[85] R. Kandel, S.R. Jang, U. Ghimire, S. Shrestha, B.K. Shrestha, C.H. Park, C.S. Kim, Engineered nanostructure fibrous cell-laden biointerfaces integrating Fe_3O_4/SrO_2-fMWCNTs induce osteogenesis and anti-bacterial effect, J. Ind. Eng. Chem. 120 (2023) 216–230, doi:10.1016/j.jiec.2022.12.028.
[86] E. Wrobel, J. Leszczynska, E. Brzoska, The Characteristics of human bone-derived cells (HBDCS) during osteogenesis in vitro, Cell. Mol. Biol. Lett. 21 (2016) 26, doi:10.1186/s11658-016-0027-8.
[87] R. Xu, Effect of whey protein on the proliferation and differentiation of osteoblasts, J. Dairy Sci. 92 (2009) 3014–3018, doi:10.3168/jds.2008-1702.
[88] J. Aragoneses, N. López-Valverde, A. López-Valverde, C. Rodríguez, B. Macedo De Sousa, J.M. Aragoneses, Bone response to osteopontin-functionalized carboxyethylphosphonic acid-modified implants. experimental study in a minipig model, Front. Mater. 9 (2022), doi:10.3389/fmats.2022.914853.
[89] L. Chen, C. Wu, D. Wei, S. Chen, Z. Xiao, H. Zhu, H. Luo, J. Sun, H. Fan, Biomimetic mineralized microenvironment stiffness regulated BMSCs osteogenic differentiation through cytoskeleton mediated mechanical signaling transduction, Mater. Sci. Eng. C 119 (2021) 111613, doi:10.1016/j.msec.2020.111613.
[90] A. Michalicha, K. Pałka, A. Roguska, M. Pisarek, A. Belcarz, Polydopamine-coated curdlan hydrogel as a potential carrier of free amino group-containing molecules, Carbohydr. Polym. 256 (2021) 117524, doi:10.1016/j.carbpol.2020.117524.
[91] Z. Wu, K. Yuan, Q. Zhang, J.J. Guo, H. Yang, F. Zhou, Antioxidant PDA-PEG nanoparticles alleviate early osteoarthritis by inhibiting osteoclastogenesis and angiogenesis in subchondral bone, J. Nanobiotechnology. 20 (2022) 479, doi:10.1186/s12951-022-01697-y.